# THE METHOD OF FICTITIOUS SOURCES APPLIED TO DIFFRACTION GRATINGS

**G. Tayeb**

Laboratoire d'Optique Electromagnétique, Unité de Recherche Associée au CNRS N. 843
Faculté des Sciences et Techniques de Saint Jérôme (Case 262), 13397 MARSEILLE Cedex 20, FRANCE

*ABSTRACT. This paper deals with grating diffraction in electromagnetic theory, using the method of fictitious sources. We present a detailed description of the method, and we lay stress on its numerical implementation. Numerical examples are given for various grating profiles, and compared to those obtained with other methods. An efficient method for the computation of the Green's function for gratings and its derivatives is given.*

## 1. INTRODUCTION

The method of fictitious sources (MFS) relies upon a simple idea: the electromagnetic field in the different domains of the structure is expressed as a combination of fields radiated by adequate sources. These sources have no physical existence, and this is why we call them "fictitious" sources. In other words, we can say that they generate electromagnetic fields which form convenient bases for the actual field. From a numerical point of view, proper bases are those capable of representing the solution with the fewest number of functions. Obviously, the quality of the bases is closely linked with the nature of the sources and their location. This fact entails one of the most problematic features in the numerical implementation: how to choose between the infinite possibilities of fictitious sources? In this paper, we try to give some basic answer elements to this question, and we present results for various shapes of gratings. Two kinds of sources have been implemented. They are both described, but we only give results for the wire sources that we found more adequate.

Another difficult subject is the computation of the field radiated by the sources. For our purpose, we need to compute the Green's function for gratings [1] with good accuracy and reasonable computer time. This Green's function is expressed in series, and their direct summation converges extremely slowly. The algorithm used in order to enhance the convergence rate of the Green's function and its gradient is described in section 4.

We began our study with this method a few years ago, both from a theoretical [2, 3] and from a numerical [3, 4] point of view. At the same time, two other groups have worked on the same basic ideas [5, 6, 7, 8, 9, 10]. Because their approaches are different from ours, it seems interesting to compare our results to those concerning gratings of cylinders, echelette gratings, and sinusoidal gratings published in these papers. Some comparisons with a code using an integral method are also performed.

## 2. THE MFS ALGORITHM

In this section, our purpose is to give an outline of the basic scheme of the MFS. We only lay stress on the implementation of the algorithm, and for more theoretical considerations, the reader can report to references [2, 3].

### 2.1 Notations

For the sake of simplicity, let us first consider the case of the ruled grating depicted in Figure 1. The grating surface $y = f(x)$ is z-independent. Function $f(x)$ is periodic, and its period $d$ is the grating pitch. Because all the electromagnetic functions involved in the solution of the problem are pseudo-periodic [1], it is sufficient to consider only one period of the grating. We call "grating profile" the curve $\mathscr{P}$ which is the graph of $f(x)$ for $0 < x < d$. The superstrate $\Omega_1$ is the region $y > f(x)$, filled with a material whose real permittivity is $\varepsilon_1 = \nu_1^2$. The substrate $\Omega_2$ is the region $y < f(x)$. It is filled with a material whose complex permittivity is $\varepsilon_2 = \nu_2^2$.

Throughout the paper, we assume a time dependence in $\exp(-i\omega t)$, and the grating is illuminated under the incidence $\theta$ by a plane wave. We only consider the two fundamental cases of polarization called E// or H// depending on whether the electric field or the magnetic field is parallel to the z axis. Therefore, the incident field as well as the total field can be represented by scalar complex functions $u^i(x,y)$ and $u(x,y)$, namely the z component of the electric or magnetic field depending on the polarization. Denoting by $\varepsilon_0$ and $\mu_0$ the permittivity and the permeability of the vacuum, we put $k_0 = 2\pi/\lambda = \omega(\varepsilon_0\mu_0)^{1/2}$, $k_1 = k_0 \nu_1$, $k_2 = k_0 \nu_2$. Putting

$$\alpha_0 = k_1 \sin\theta \tag{1}$$

and $\beta_0 = k_1 \cos\theta$, the incident field can be expressed as:

$$u^i(x,y) = \exp(i\alpha_0 x - i\beta_0 y) \tag{2}$$

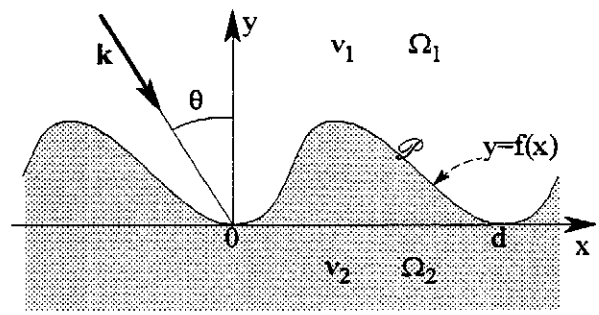


*Figure 1*

### 2.2 Unknowns

We search the total field $u(x,y)$ in each region of space. For convenience, let us define in $\Omega_1$ the diffracted field $u^d(x,y)$ as the difference:

$$u^d(x,y) = u(x,y) - u^i(x,y) \tag{3}$$

Noting that the incident field verifies in whole space:

$$\Delta u^i + k_1^2 u^i = 0 \quad , \tag{4}$$

the solution must fulfil the following requirements:

a) $\Delta u^d + k_1^2 u^d = 0 \qquad \text{in } \Omega_1$ , (5)

b) $\Delta u + k_2^2 u = 0 \qquad \text{in } \Omega_2$ , (6)

c) a radiation condition for $u^d$ in $\Omega_1$ and for u in $\Omega_2$ , (7)

d) the boundary conditions on the grating surface for the total field and its normal derivative:

$$u^+ = u^- = u(x,f(x)) \tag{8}$$

$$p^+ Du^+ = p^- Du^- \tag{9}$$

where

- Du stands for the normal derivative of u on $\mathscr{P}$,
- superscripts + (or -) in u and Du stand for the limit values obtained when the fields are taken in $\Omega_1$ (or $\Omega_2$),
- coefficients $p^+$ and $p^-$ are both equal to 1 in E// polarization, and are equal to $1/\varepsilon_1$ and $1/\varepsilon_2$ in H// polarization.

Using (3), the boundary conditions (8) and (9) on $\mathscr{P}$ can also be written as:

$$u^i(x,f(x)) + u^d(x,f(x)) = u(x,f(x)) \tag{8'}$$

$$p^+ Du^i + p^+ Du^d = p^- Du^- \tag{9'}$$

Due to the radiation condition, the fields $u^d(x,y)$ in $\Omega_1$ and $u(x,y)$ in $\Omega_2$ can be expressed in an integral form from their values on $\mathscr{P}$ and from the value of their normal derivatives on $\mathscr{P}$ (Kirchhoff-Helmholtz formula) [1, 11]. At the present time, we only need to notice that the problem reduces to the search of the two functions u(x,f(x)) and $p^+ Du^+ = p^- Du^-$ defined on $\mathscr{P}$.

From what precedes, it appears that we can characterize the fields by columns defined on $\mathscr{P}$, and we put:

$$F^i = \begin{vmatrix} u^i(x,f(x)) \\ p^+ Du^i \end{vmatrix} , \quad F^d = \begin{vmatrix} u^d(x,f(x)) \\ p^+ Du^d \end{vmatrix} , \quad F = \begin{vmatrix} u(x,f(x)) \\ p^- Du^- \end{vmatrix} \tag{10}$$

The boundary conditions can now be written as:

$$F^i + F^d = F \tag{11}$$

and it is worth noting that $F^d$ represents limit values on $\mathscr{P}$ of the diffracted field in $\Omega_1$, whereas F represents limit values on $\mathscr{P}$ of the total field. Note that the total field is also the diffracted field in $\Omega_2$.

### 2.3 Expansions of the fields

In the domain $\Omega_2$, the total field u(x,y) must satisfy the Helmholtz equation (6) and a radiation condition. It can be expressed as an adequate combination of an infinite set of fields $e_{2,n}(x,y)$ which verify these two requirements. We can choose for $e_{2,n}(x,y)$ the field radiated by a fictitious source located in $\Omega_1$, supposing that the whole space is filled by a material of permittivity $\varepsilon_2$. This source is represented by a pseudo-periodic distribution $S_{2,n}$ whose support is in $\Omega_1$. Because this elementary field $e_{2,n}$ satisfies

$$\Delta e_{2,n} + k_2^2 e_{2,n} = S_{2,n} \tag{12}$$

it also verifies (6). In the same way, $u^d(x,y)$ will be expressed as a combination of fields $e_{1,n}(x,y)$ radiated by fictitious sources $S_{1,n}$ located in $\Omega_2$, supposing that the whole space is filled by a material of permittivity $\varepsilon_1$:

$$\Delta e_{1,n} + k_1^2 e_{1,n} = S_{1,n} \tag{13}$$

Let us define the columns:

$$F_{1,n} = \begin{vmatrix} e_{1,n}(x,f(x)) \\ p^+ De_{1,n} \end{vmatrix} , \quad F_{2,n} = \begin{vmatrix} e_{2,n}(x,f(x)) \\ p^- De_{2,n} \end{vmatrix} . \tag{14}$$

From a practical point of view, the problem can be summarized in the following way: find the coefficients $c_{1,n}$ and $c_{2,n}$ (the complex amplitudes of the sources $S_{1,n}$ and $S_{2,n}$) in order to fulfil the boundary conditions:

$$F^i + \sum_n c_{1,n} F_{1,n} = \sum_n c_{2,n} F_{2,n} \tag{15}$$

The solution will further be given by

$$u^d(x,y) = \sum_n c_{1,n} e_{1,n}(x,y) \qquad \text{in } \Omega_1 \tag{16}$$

$$u(x,y) = \sum_n c_{2,n} e_{2,n}(x,y) \qquad \text{in } \Omega_2 \tag{17}$$

This simple presentation hides difficult problems of functional analysis. The interested reader will find in references [2, 3] more information about the functional spaces in which F columns lie, about the way to get total families $F_{1,n}$ and $F_{2,n}$ in these spaces, about the subjacent notion of convergence, etc...

### 2.4 Least squares minimization

For the numerical implementation, we will retain a finite number N of basis functions, i.e. N fictitious sources for the expansions (16) and (17). Due to this truncature, equation (15) will not be exactly fulfilled, and we use a least squares technique to find the coefficients $c_{1,n}(N)$ and $c_{2,n}(N)$ which give the following norm its minimum value $\Delta_N$:

$$\Delta_N = \min \left\| F^i + \sum_{n=1,N} c_{1,n}(N) F_{1,n} - \sum_{n=1,N} c_{2,n}(N) F_{2,n} \right\| \tag{18}$$

This norm is induced by the scalar product $(F|F')$ of two columns F and F' defined on $\mathscr{P}$:

$$F = \begin{vmatrix} u \\ v \end{vmatrix} , \qquad F' = \begin{vmatrix} u' \\ v' \end{vmatrix} , \tag{19}$$

$$(F|F') = \int_{\mathscr{P}} (u\,\bar{u}' + \partial_t u\, \partial_t \bar{u}' + v\,\bar{v}')\, d\ell \quad , \tag{20}$$

where $\partial_t$ stands for the tangential derivative on $\mathscr{P}$, and $\ell$ is the curvilinear abscissa. In the numerical implementation, it appears useful to give appropriate weights to the different terms of the norm and we take:

$$\begin{aligned} \|F\|^2 &= w_1 \int_{\mathscr{P}} |u|^2 d\ell + w_2 \int_{\mathscr{P}} |\partial_t u|^2 d\ell + w_3 \int_{\mathscr{P}} |v|^2 d\ell \\ &\overset{\text{def}}{=} w_1 \mathcal{N}_1(F) + w_2 \mathcal{N}_2(F) + w_3 \mathcal{N}_3(F) \end{aligned} \tag{21}$$

The choice of the three positive constants $w_1$, $w_2$ and $w_3$ is of great importance in the efficiency of the numerical

process. Indeed, equation (14) shows that the two components of any column F are generally not of the same order of magnitude. The ratio between these two components depends on numerous parameters such as the spatial variations of the fields (through the spatial derivatives, which are themselves linked with the wavelength, the location of the fictitious sources, the permittivities), the polarization and the permittivities $\varepsilon_1$ and $\varepsilon_2$ (through the parameters $p^+$ and $p^-$). Many numerical experiments have been done in order to determine a convenient way to choose these weights. Obviously, there is no perfect and general solution, and at the present time, our computer code uses the following recipes:

- We take $w_1 = 1$
- The second term containing the tangential derivative in (20) or (21) results from theoretical considerations detailed in [2]. The numerical experiments that we have performed have shown that this term is of minor importance in most computations. Therefore, all the numerical examples given in this paper are computed taking $w_2 = 0$. But it is worth noting that, because this term contains tangential derivatives, it could be interesting to take it into consideration in the minimization process in the case where the solution would exhibit spurious tangential variations.
- The weight $w_3$ is computed from the values of $F_{1,n}$ and $F_{2,n}$ in a way which gives approximately, and whatever the parameters (wavelength, location of sources, polarization, permittivities), the same importance in the norm to the two terms $\mathcal{N}_1$ and $\mathcal{N}_3$ (Eq. (21)). This is achieved by taking:

$$w_3 = \frac{\sum_{n=1,N} \int_{\mathscr{P}} \left[ \left|e_{1,n}\right|^2 + \left|e_{2,n}\right|^2 \right] d\ell}{\sum_{n=1,N} \int_{\mathscr{P}} \left[ \left|p^+ De_{1,n}\right|^2 + \left|p^- De_{2,n}\right|^2 \right] d\ell} \qquad (22)$$

where (referring to (14) and (21)), the numerator (resp. denominator) is the sum over all the basis functions of the first term $\mathcal{N}_1$ (resp. $\mathcal{N}_3$).

In the numerical implementation, all the integrals on $\mathscr{P}$ are performed with the simple rectangular rule, and we denote by $N_d$ the number of sampling points. With that choice, the size of the matrix involved in the least squares problem is $2N_d \times 2N$. In the numerical examples of section 3, the ratio $N_d/N$ is taken equal to 1.5 or 2.

One of the important features of the MFS is that the least squares minimization process gives an estimation of the accuracy of the solution. Referring to (18), let us define a normalized error $\Delta$ as:

$$\Delta = \frac{\Delta_N}{\|F_i\|} \qquad (23)$$

Although it seems impossible to find a rigorous quantitative relationship between $\Delta$ and the accuracy of the solution, it appears that the value of $\Delta^2$ generally gives a good idea of the accuracy of the diffracted efficiency in each order (see section 3.3). This is why $\Delta^2$ will be reported in the numerical examples of section 3. This feature is quite interesting from a practical point of view. Indeed, it enables one to dispense with time consuming convergence tests.

### 2.5 The grating Green's function

Let us consider the "pseudo-periodic Dirac distribution for gratings" [1]:

$$\delta_{\mathscr{G}}(x,y) = \sum_{m\in Z} \delta(y)\, \delta(x - md) \exp(im\alpha_0 d) \qquad (24)$$

The pseudo-periodic solution $g_k(x,y)$ (subscript k recalls the optical parameter $k = \omega (\varepsilon\mu)^{1/2}$ of the medium) of the equation

$$\Delta g_k + k^2 g_k = \delta_{\mathscr{G}}, \qquad (25)$$

which satisfies a radiation condition for $y \to \pm\infty$, is the so-called grating Green's function [1]:

$$g_k(x,y) = \frac{1}{2id} \sum_{m\in Z} \frac{1}{\beta_m} \exp(i\alpha_m x + i\beta_m |y|) \qquad (26)$$

where

$$\alpha_m = \alpha_0 + m\,2\pi/d \qquad (27)$$

$$\beta_m{}^2 = k^2 - \alpha_m{}^2 \qquad (28)$$

with $\beta_m$ being chosen in such a way that its imaginary part is positive.

### 2.6 Fictitious sources and basis functions

In order to get the total families $F_{1,n}$ and $F_{2,n}$, we must choose convenient sources $S_{1,n}$ and $S_{2,n}$. We have used two kinds of sources (wire sources and continuous sources), which are described below.

We first focus on the determination of columns $F_{1,n}$. We consider (Figure 2) a periodic curve (with period d) located in $\Omega_2$, and define $\mathscr{R}_1$ as the first period ($0 \le x < d$) of this curve.

*Wire sources:*

Let us consider a point $P_{1,n}$ with co-ordinates $(x_{1,n}, y_{1,n})$ on $\mathscr{R}_1$. According to (13), (24) and (25), the source

$$S_{1,n} = \delta_{\mathscr{G}}(x - x_{1,n}, y - y_{1,n}) = \sum_{m\in Z} \delta(y - y_{1,n})\, \delta(x - x_{1,n} - md) \exp(im\alpha_0 d) \qquad (29)$$

gives rise to the elementary field:

$$e_{1,n}(x,y) = g_{k_1}(x - x_{1,n}, y - y_{1,n}) \qquad (30)$$

This field $e_{1,n}$ possesses an intuitive physical interpretation. Indeed, it can be considered as the field radiated in the whole space filled with material of permittivity $\varepsilon_1$ by an array of currents flowing in infinitely thin wires. These wires are parallel to the z axis, and intersect the (x,y) plane at points $(x_{1,n} + md, y_{1,n})$.

The column $F_{1,n}$ associated with $S_{1,n}$ is then given by (14) from the knowledge of the Green's function and its gradient. Finally, the set of columns $F_{1,n}$ (n=1, N) is

obtained through the choice of a layout of N points $P_{1,n}$ on the curve $\mathscr{P}_1$.

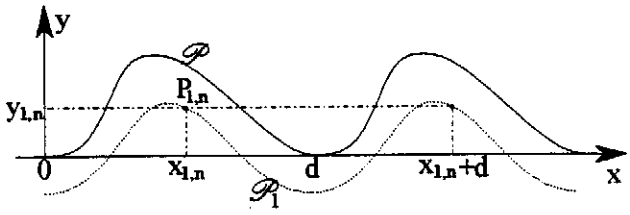


*Figure 2. The value of* $x_{1,n}$ *is in* [0,d[.

***Continuous sources:***
These sources are characterized by a pseudo periodic distribution whose support is $\mathscr{P}_1$. Denoting by $\ell_1$ the curvilinear abscissa on $\mathscr{P}_1$ and by $L_1$ the length of one period of $\mathscr{P}_1$, $S_{1,n}$ is defined on the first period ($0 \le x < d$) by:

$$S_{1,n} = \exp(in2\pi\,\ell_1 / L_1)\,\delta_{\mathscr{P}_1} \tag{31}$$

and gives rise (Eq. (13)) to the elementary field:

$$e_{1,n}(x,y) = \int_{\mathscr{P}_1} e^{in2\pi\ell_1/L_1}\, g_{k_1}\big(x - x_1(\ell_1), y - y_1(\ell_1)\big)\, d\ell_1 \tag{32}$$

where $x_1(\ell_1)$ and $y_1(\ell_1)$ are the co-ordinates of the point going along $\mathscr{P}_1$. The second component of the column $F_{1,n}$ associated with $S_{1,n}$ is given by the integral:

$$De_{1,n}(x,f(x)) = \int_{\mathscr{P}_1} e^{in2\pi\ell_1/L_1}\, Dg_{k_1}\big(x - x_1(\ell_1), f(x) - y_1(\ell_1)\big)\, d\ell_1 \tag{33}$$

Integrals (32) and (33) are computed by Gaussian quadrature, using Gauss-Legendre polynomials [12]. We finally get the set of N columns $F_{1,n}$ (we assume here that N=2P+1 is an odd number) by taking n between -P and P. From Eq. (31), these sources can be interpreted as continuous surface currents flowing on $\mathscr{P}_1$; their harmonic variations become quicker as n increases.

The determination of columns $F_{2,n}$ is performed in the same way, using a curve $\mathscr{P}_2$ located in $\Omega_1$, and taking the Green's function $g_{k_2}$ (associated with the medium that fills the substrate).

It is worth noting that, to our knowledge, theoretical considerations cannot predict how fast the convergence of the algorithm is with respect to the number of sources N. Indeed, we can expect to improve the rapidity of convergence by a good choice of curves $\mathscr{P}_1$ and $\mathscr{P}_2$, and, in the case of wire sources, by a convenient layout of points $P_{1,n}$ and $P_{2,n}$ on these curves. The numerous possibilities in these choices make the method powerful, but, on the other hand, make the programmer's work difficult. The examples of section 3 give some light on this subject.

From our experiments, we found the wire sources more convenient than the continuous sources. In the case of complex shaped gratings, they are easier to handle (their location can be done automatically from the sampling points on $\mathscr{P}$, whereas the continuous sources need an explicit definition of curves $\mathscr{P}_1$ and $\mathscr{P}_2$). Except for the echelette grating, all the examples given in section 3 have been tested with both kinds of sources. For each of them, the wire sources give more accurate results with less computation time. This is why, in section 3, we only present results with the wire sources.

### 2.7 Infinitely conducting materials

The case of an infinitely conducting substrate is solved in the same way. In this case, the sources $S_{2,n}$ vanish, and the number of unknowns is divided by two (just put $c_{2,n} = 0$ in Eq. (15)).
When dealing with a dielectric or a lossy grating, it often appears interesting to also consider the case of an infinitely conducting grating. Indeed, it needs very little additional numerical effort (since the columns $F_{1,n}$ have already been computed), and it can give supplementary information and checking (through the energy balance, for instance).

### 2.8 Computation of the efficiencies

The diffracted efficiencies are obtained from the amplitudes $c_{1,n}$ and $c_{2,n}$ of the sources. For instance, in the case of wire sources, Eqs. (16), (30) and (26) give the Rayleigh expansion of the diffracted field in $\Omega_1$:

$$u^d(x,y) = \sum_{m\in\mathbb{Z}} R_m \exp(i\alpha_m x + i\beta_m y) \tag{34}$$

where the Rayleigh coefficient $R_m$ is given by:

$$R_m = \frac{1}{2id\,\beta_{1,m}} \sum_{n=1,N} c_{1,n} \exp(-i\alpha_m x_{1,n} - i\beta_{1,m} y_{1,n}) \tag{35}$$

In the same way, the Rayleigh coefficients of the transmitted field in $\Omega_2$ are:

$$T_m = \frac{1}{2id\,\beta_{2,m}} \sum_{n=1,N} c_{2,n} \exp(-i\alpha_m x_{2,n} + i\beta_{2,m} y_{2,n}) \tag{36}$$

From these Rayleigh coefficients, the calculation of the efficiencies is straightforward.

## 3. Numerical results

We give in this section some numerical results for various shapes of gratings. We compare our data with those given in [6, 7, 8], and also give new ones.

In order to check the accuracy of the computations, we report the square of the normalized error $\Delta^2$ defined by (23). We also report the sum $\Sigma$ of all the diffracted efficiencies. This sum must be equal to unity when all the materials are lossless.

We denote by T the computation time for both polarizations cases (E// and H//) on an IBM RS/6000 workstation using a PowerPC 601 processor (about 13 MFlops).

### 3.1 Sinusoidal grating

The grating profile is described by:

$$y = f(x) = \frac{h}{2}\left(1+\cos\left(\frac{2\pi x}{d}\right)\right) \qquad (37)$$

Let us consider the following data: $d = 3.9\,\lambda$, $h = 0.5\,\lambda$, $\varepsilon_1 = \varepsilon_0$, $\varepsilon_2 = 3\,\varepsilon_0$, $\theta = 30°$. We use $N = 30$ wire sources on the lines $\mathscr{P}_1$ and $\mathscr{P}_2$ described by:

$$f_1(x) = f(x) - e_1 \quad \text{and} \quad f_2(x) = f(x) + e_2 \qquad (38)$$

with $e_1 = e_2 = 0.375\,\lambda$. These sources are equally spaced in the x direction (Figure 3).

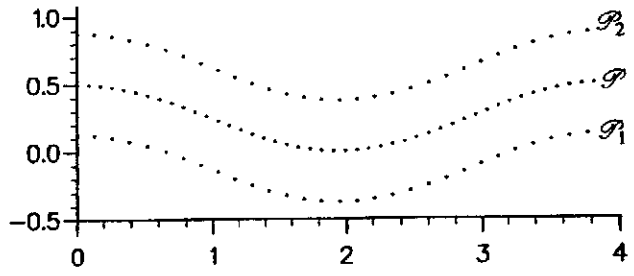


*Figure 3. The dots on $\mathscr{P}_1$ and $\mathscr{P}_2$ show the location of the sources. The dots on $\mathscr{P}$ show the $N_d$ sampling points used in the least squares problem. Dimensions are given in units of $\lambda$.*

Table 1 gives the diffracted efficiencies and the energy balance $|\Sigma-1|$, which are compared with those given by Boag et al. in [8]. The most significant differences between their method and ours are:

- in [8], the sources are strips instead of wires,
- in [8], the boundary conditions are imposed on a number of points which give a square system of linear equations, whereas we use more sampling points and a least squares algorithm.

The results are in perfect agreement. It must be noticed that, because this grating profile is very smooth, we easily obtain a high accuracy. The computation time for Table 1 is T = 21s for both polarizations. By reducing the number of sources from N = 30 to N = 15, we still get 4 exact digits on each efficiency, and T falls to 3s.

Let us consider (Figure 4) a deep metallic sinusoidal grating, with $d = 0.8333333$ µm, $h = 0.8$ µm, $\varepsilon_1 = \varepsilon_0$, $\nu_2 = 1.3 + i\,7.1$ (aluminium), $\lambda = 0.6$ µm, $\theta = 0°$.

In the case of such deep gratings, numerical experiments have shown that taking for $\mathscr{P}_1$ and $\mathscr{P}_2$ lines translated from $\mathscr{P}$ (as in Eq. (38)), and taking the

| | E// | | H// |
|---|---|---|---|
| | From ref. [8] | MFS | MFS |
| $e_{r,-5}$ | 0.000045851 | 0.000045852 | 0.000047376 |
| $e_{r,-4}$ | 0.0011340 | 0.001134006 | 0.001234301 |
| $e_{r,-3}$ | 0.0080707 | 0.008070730 | 0.008229349 |
| $e_{r,-2}$ | 0.020802 | 0.020802137 | 0.018170862 |
| $e_{r,-1}$ | 0.012813 | 0.012812680 | 0.008577814 |
| $e_{r,0}$ | 0.0029595 | 0.002959457 | 0.001316383 |
| $e_{r,1}$ | 0.050775 | 0.050775064 | 0.008784567 |
| $e_{t,-8}$ | 0.000000010 | 0.000000010 | 0.000000009 |
| $e_{t,-7}$ | 0.000000027 | 0.000000027 | 0.000000032 |
| $e_{t,-6}$ | 0.000000003 | 0.000000003 | 0.000000007 |
| $e_{t,-5}$ | 0.000000069 | 0.000000069 | 0.000000097 |
| $e_{t,-4}$ | 0.000015240 | 0.000015240 | 0.000022144 |
| $e_{t,-3}$ | 0.0010135 | 0.001013501 | 0.001271741 |
| $e_{t,-2}$ | 0.022739 | 0.022738876 | 0.026661619 |
| $e_{t,-1}$ | 0.18653 | 0.186525791 | 0.215598073 |
| $e_{t,0}$ | 0.33415 | 0.334153259 | 0.412516658 |
| $e_{t,1}$ | 0.33666 | 0.336658394 | 0.278727999 |
| $e_{t,2}$ | 0.016407 | 0.016407201 | 0.018145503 |
| $e_{t,3}$ | 0.0045496 | 0.004549572 | 0.000479686 |
| $e_{t,4}$ | 0.0013381 | 0.001338132 | 0.000215810 |
| $\|\Sigma-1\|$ | 0.17 E-6 | 0.10 E-8 | 0.31 E-7 |
| $\Delta^2$ | | 0.36 E-10 | 0.12 E-10 |

*Table 1. Reflected $e_{r,n}$ and transmitted $e_{t,n}$ efficiencies in order n for the grating of Figure 3.*

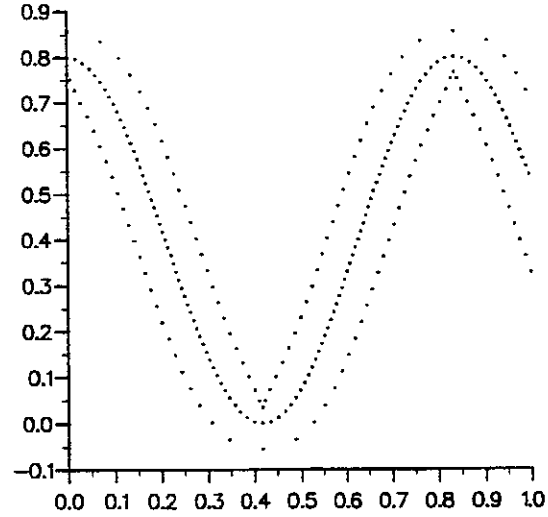


*Figure 4. Deep metallic sinusoidal grating. In this case, N = 50, and $N_d$ = 100.*

*Table 2*

| | N | E// | | | H// | | | T |
|---|---|---|---|---|---|---|---|---|
| | | $e_{r,0}$ | $e_{r,1} = e_{r,-1}$ | $\Delta^2$ | $e_{r,0}$ | $e_{r,1} = e_{r,-1}$ | $\Delta^2$ | |
| MFS | 40 | .178 | .310 | .58 E-2 | .369 | .164 | .93 E-3 | 31 s |
| | 50 | .1791 | .3140 | .18 E-2 | .37063 | .16485 | .18 E-3 | 48 s |
| | 70 | .18013 | .31548 | .20 E-3 | .37099 | .16490 | .11 E-4 | 97 s |
| | 80 | .180070 | .315527 | .74 E-4 | .371136 | .164888 | .39 E-5 | 127 s |
| | 100 | .180104 | .315558 | .13 E-4 | .371158 | .164913 | .78 E-6 | 207 s |
| | 120 | .180162 | .315584 | .36 E-5 | .371156 | .164908 | .25 E-6 | 309 s |
| Integral method | 80 | .171 | .313 | | .384 | .165 | | 4 s |
| | 120 | .1775 | .3148 | | .3745 | .1648 | | 10 s |
| | 150 | .17886 | .31521 | | .37267 | .16483 | | 17 s |
| | 200 | .17972 | .31547 | | .37160 | .16481 | | 36 s |
| | 300 | .18012 | .31559 | | .37111 | .16481 | | 100 s |

sampling points and the sources equally spaced in the x direction, do not give a fast convergence of the results with respect to N.

We have developed routines that automatically give regularly spaced points on $\mathscr{P}$, and choose the position of the N sources from the position of the $N_d$ sampling points and from the radius of curvature of $\mathscr{P}$, with $N = N_d/2$. These points are depicted in Figure 4.

Table 2 shows the results obtained for this grating. They are compared to those given by a computer code using an integral method and built by D. Maystre [13]. In Table 2, N stands for the number of sources in the case of the MFS, and also stands for the number of sampling points on the grating profile used for the discretization of the integral equations in the case of the integral method. For this example, the computations are faster with the integral method. But the conclusion could be different for other gratings. In fact, we have not performed extensive comparisons between the two methods. We can only say that for sinusoidal gratings with not so deep grooves, the computation times are equivalent for the two methods. There are also some gratings which can be handled by the MFS and not by the integral method (see section 3.4).

### 3.2 Echelette grating

Let us consider (Figure 5a) a lossless echelette grating with the same opto-geometrical parameters as in Ref. [7]: d = 1.25 μm, total depth h = 0.625 μm, blazing angle 45°, $\varepsilon_1 = \varepsilon_0$, $\varepsilon_2 = 3\,\varepsilon_0$, λ = 0.546 μm, θ = 15°.

Because our numerical implementation needs the normal derivative of the fields on $\mathscr{P}$, the actual grating profile is replaced by its truncated Fourier series, in which we keep 40 harmonics. The new profile so obtained has no edges and is very close to the actual one. Of course, we have checked the convergence of the results when the number of harmonics increases.

Table 3 gives the diffracted efficiencies and the energy balance. The computation time is T = 25s for both polarizations. By reducing the number of sources from N = 50 to N = 30, the biggest change over all the efficiencies is equal to 3 E-3, and T is reduced to 9s.

| | E// | | H// |
|---|---|---|---|
| | From ref. [7] | MFS | MFS |
| $e_{r,-2}$ | 0.0053 | 0.00538 | 0.00067 |
| $e_{r,-1}$ | 0.0219 | 0.02170 | 0.00041 |
| $e_{r,0}$ | 0.0009 | 0.00079 | 0.00022 |
| $e_{r,1}$ | 0.0009 | 0.00091 | 0.00085 |
| $e_{t,-4}$ | 0.0243 | 0.02416 | 0.00616 |
| $e_{t,-3}$ | 0.0087 | 0.00875 | 0.00428 |
| $e_{t,-2}$ | 0.1588 | 0.15837 | 0.17379 |
| $e_{t,-1}$ | 0.1307 | 0.13096 | 0.20990 |
| $e_{t,0}$ | 0.0025 | 0.00235 | 0.03375 |
| $e_{t,1}$ | 0.5022 | 0.50328 | 0.48732 |
| $e_{t,2}$ | 0.0948 | 0.09479 | 0.07654 |
| $e_{t,3}$ | 0.0486 | 0.04866 | 0.00679 |
| \|Σ-1\| | 0.2 E-3 | 0.9 E-4 | 0.6 E-3 |
| $\Delta^2$ | | 0.4 E-7 | 0.2 E-5 |

*Table 3. Efficiencies for the grating of Figure 5a.*

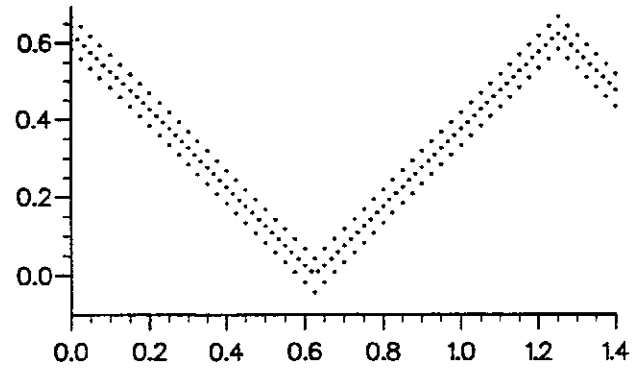


*Figure 5a. Dielectric echelette grating. In this case, N = 50, and $N_d$ = 75.*

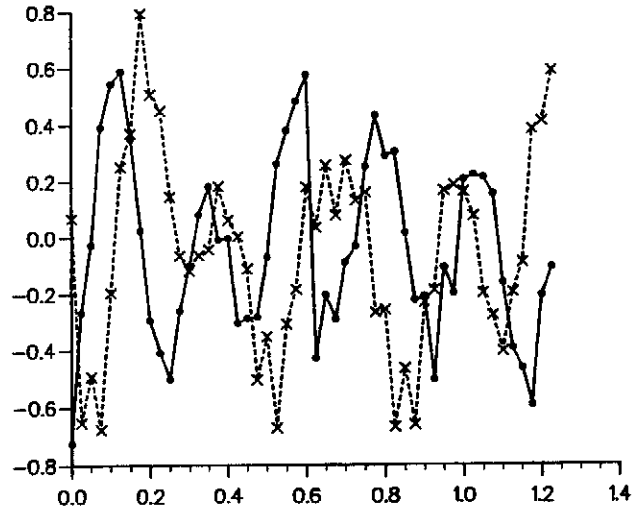


*Figure 5b. Real part (solid line) and imaginary part (dashed line) of the $c_{1,n}$ coefficients versus the actual abscissa of the sources. E// polarization.*

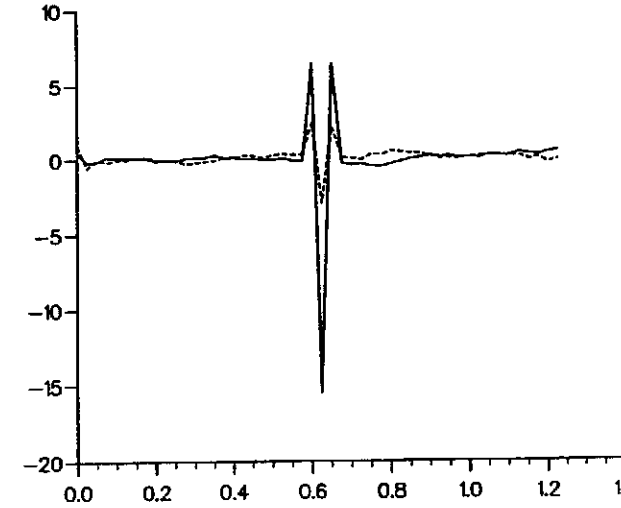


*Figure 5c. Same as Fig. 5b, but for H// polarization.*

The comparison with results of [7] shows once more a perfect agreement. The most significant differences between the two methods are the same as in the preceding section.

Figures 5b and 5c give for both polarizations the real

part (solid line) and the imaginary part (dashed line) of the complex amplitudes $c_{1,n}$ of the sources $S_{1,n}$ radiating the diffracted field in $\Omega_1$ (Eq. (16)). It can be observed that in the H// case, these amplitudes are much greater near the protruding edges. This fact has already been emphasized in [4]. It becomes less marked when the sources are placed closer to the profile. Boag et al. have used some additional sources near the edges in order to get a better representation of the field near these points. We have not used an improvement like this.

### 3.3 Grating of cylinders

For this kind of grating (Figure 6), there are some minor changes in comparison with the method described in section 2. The sources which create the diffracted field are inside the cylinders, and those which create the field inside the cylinders are outside. The boundary conditions lead to integrals on the cylinder surfaces.

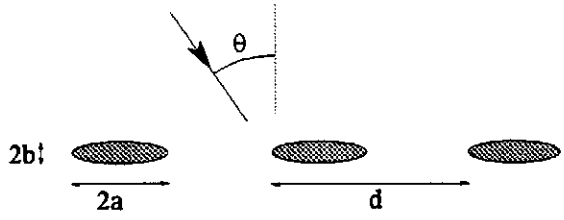


*Figure 6.*

The case of circular cylinders (a=b) is generally easy to solve. We have compared our results to those given in Ref. [6] for infinitely conducting cylinders. Once more, the agreement is perfect: using the same number of wire sources as Boag et al., we find exactly the same 5 digits for all the efficiencies given in Table 1 of [6].

In the case of flattened elliptic cylinders, the location of the sources assumes a greater importance. It appears interesting to put more sources near the regions of high radius of curvature. An example is given in Figure 7 for a grating of metallic cylinders lying in vacuum, with the opto-geometrical parameters: $d = 0.5$, $a = 0.12$, $b = 0.03$, $\varepsilon_1 = \varepsilon_0$, optical index of the cylinders $\nu_2 = 1.3 + i\,7.1$, $\lambda = 0.5$, $\theta = 45°$.

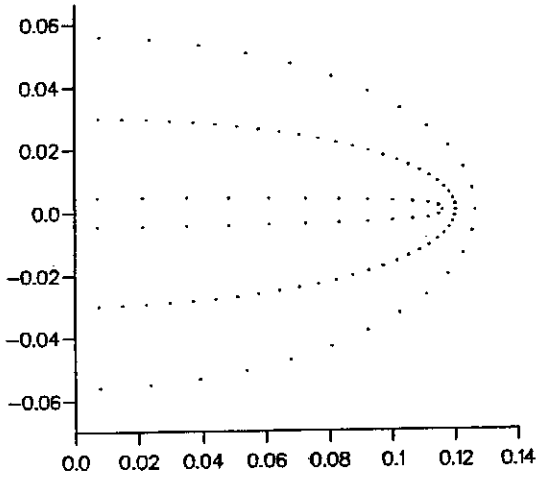


*Figure 7. Wire sources and sampling points used in the computation ($N = 50$, $N_d = 2N$). Only one half of the cylinder is shown.*

Table 4 shows, in E// polarization, the convergence of the solution versus the number N of sources. The reflected efficiencies in 0 and -1 order, the sum $\Sigma$ of all the diffracted efficiencies, the normalized error $\Delta^2$ and the computation time T are reported. From these data, we get the curves of Figure 8, which clearly show that the accuracy of each efficiency is closely linked with $\Delta^2$. In Figure 8, the number of accurate digits is defined by the quantity (given here for $e_{r,0}$):

$$-\log_{10}\left|\frac{e_{r,0}(N)-e_{r,0}(50)}{e_{r,0}(50)}\right| \qquad (39)$$

| N | $e_{r,-1}$ | $e_{r,0}$ | $\Sigma$ | $\Delta^2$ | T |
|---|---|---|---|---|---|
| 20 | .2014319 | .4112815 | 0.9331414 | 1.02E-03 | 6s |
| 25 | .1953378 | .4093119 | 0.9286433 | 8.92E-04 | 11s |
| 30 | .1958446 | .4095595 | 0.9294215 | 3.05E-05 | 19s |
| 35 | .1958564 | .4095748 | 0.9294324 | 8.54E-06 | 30s |
| 40 | .1958586 | .4095772 | 0.9294456 | 3.29E-06 | 48s |
| 45 | .19585927 | .40958086 | 0.92944840 | 1.66E-06 | 71s |
| 50 | .19585898 | .40958116 | 0.92944824 | 7.91E-07 | 106s |

*Table 4*

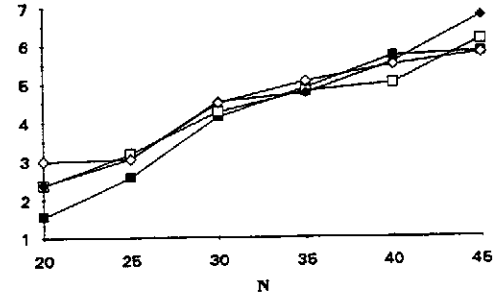


*Figure 8. The symbols ■, □, and ◆ give respectively the number of accurate digits for $e_{r,-1}$, $e_{r,0}$, and $\Sigma$, whereas the symbols ◊ represent $-\log_{10}(\Delta^2)$.*

### 3.4 Coated gratings

Let us consider a grating covered with a layer. In this case, we use two supplementary sets of sources in order to represent the electromagnetic field in the coating. These sets are placed above and below the coating (lines $\mathscr{P}_3^+$ and $\mathscr{P}_3^-$ of Figure 9). As before, the sources placed on lines $\mathscr{P}_1$ and $\mathscr{P}_2$ generate the reflected and transmitted fields respectively. In the minimization process, the boundary conditions lead to integrals on both discontinuity surfaces.

In our Laboratory, the codes using integral methods cannot deal with thin layers (the profiles must have no interpenetration). It is worth noting that these limitations do not hold for the MFS.

We consider (Figure 9) a metallic sinusoidal grating with depth $h = 0.3$ and $d = 1$ (Eq. (37)). The coating has a constant thickness $t = 0.05$ (the two interfaces are $y = f(x)$ and $y = f(x) + t$). The optical indices are $\nu_1 = 1$

(superstrate), $\nu_2 = 1.3 + i\,7.1$ (substrate), $\nu_3 = 1.5$ (coating). We take $\lambda = 0.7$ and $\theta = 45°$.
With N = 40 sources and E// polarization, we obtain in orders -2, -1 and 0 the reflected efficiencies 0.1888, 0.3961 and 0.3005, with a normalized error $\Delta^2 = 8.4$ E-6. In H// polarization, the efficiencies are 0.6264, 0.1063 and 0.0247, with $\Delta^2 = 1.3$ E-6. The computation time is T = 62s.
These efficiencies are very close to the correct ones obtained by increasing the number of sources, which are respectively 0.1887, 0.3962, 0.3006 in E// case, and 0.6268, 0.1063, 0.0247 in H// case.

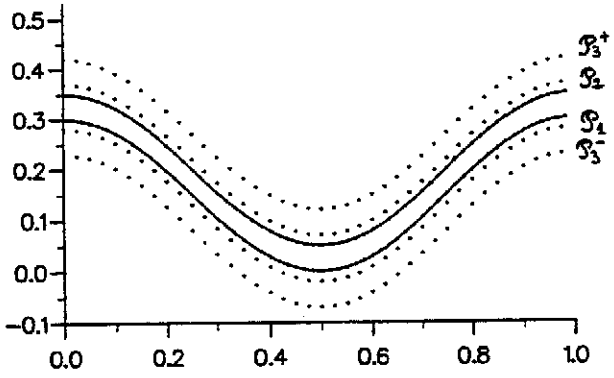


*Figure 9. The dots show the 4 sets of N=40 wire sources. The physical interfaces are in heavy lines.*

### 3.5 Grating profiles given by a parametric equation

In order to describe profiles with various shapes, we have developed some routines which smooth arbitrary profiles given by discrete points. The resulting curve is expressed as a parametric function z(t), whose real and imaginary parts give the grating profile x(t) and y(t). This is why, in this section, the grating profile is defined by a parametric equation which involves the grating pitch d, a real number $\tau$ and 2Q+1 complex numbers $C_q$ :

$$z(t) = t\frac{d}{\tau} + \sum_{q=-Q}^{Q} C_q \exp(iq2\pi\frac{t}{\tau}) \qquad (40)$$

Let us first consider (Figure 10) a deep dielectric grating whose profile is given by:
d = 5, $\tau$ = 20, Q = 3, $C_{-3} = -0.037 - i\,0.23$,
$C_{-2} = 0.17 + i\,0.4$, $C_{-1} = -0.022 - i\,1.65$, $C_0 = 0.2 + i\,4.15$,
$C_1 = -0.079 - i\,1.69$, $C_2 = -0.083 - i\,0.54$,
$C_3 = 0.079 - i\,0.025$ .
The other opto-geometrical parameters are: $\nu_1 = 1$, $\nu_2 = 1.5$, $\lambda = 4$, $\theta = 20°$.
The $N_d$ sampling points on $\mathscr{P}$ are equally spaced, and the N sources are deduced from these points, taking into account the radius of curvature of $\mathscr{P}$ (Figure 10). Table 5 shows the resulting efficiencies for this grating. The computation time is T = 45s. From computations made with a greater number of sources, we can affirm that all the digits given in Table 5 are correct.

We consider now (Figure 11) a metallic grating whose profile is given by:

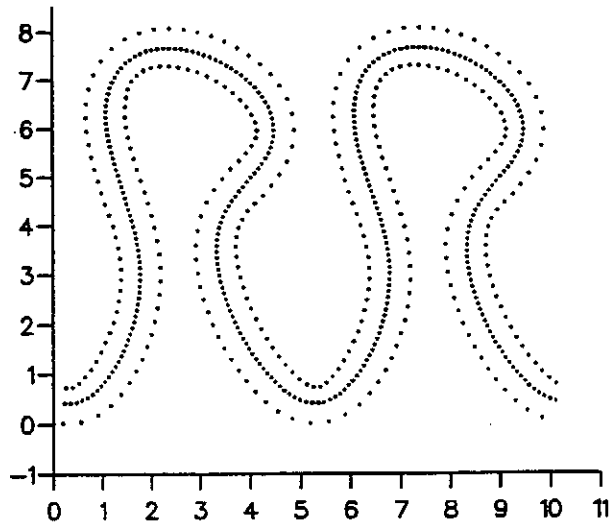


*Figure 10. Sampling points and sources for a deep dielectric grating defined by a parametric equation. $N_d$ = 150, N = 75. Two periods are shown.*

| | E// | H// |
|---|---|---|
| $e_{r,-1}$ | 0.03471 | 0.00665 |
| $e_{r,0}$ | 0.02030 | 0.00374 |
| $e_{t,-2}$ | 0.13204 | 0.05479 |
| $e_{t,-1}$ | 0.15052 | 0.73095 |
| $e_{t,0}$ | 0.08801 | 0.02686 |
| $e_{t,1}$ | 0.57441 | 0.17701 |
| $\Sigma$ | 0.999989 | 0.999998 |
| $\Delta^2$ | 1.3 E-7 | 7.6 E-8 |

*Table 5. Efficiencies for the grating of Figure 10.*

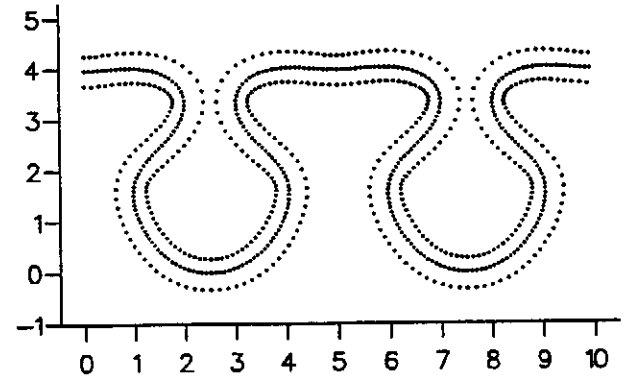


*Figure 11. Sampling points and sources for a metallic grating defined by a parametric equation. $N_d$ = 150, N = 100. Two periods are shown.*

d = 5, $\tau$ = 14.1, Q = 5, $C_{-5} = -i\,0.0488$, $C_{-4} = -i\,0.114$,
$C_{-3} = i\,0.141$, $C_{-2} = i\,0.359$, $C_{-1} = i\,1.118$, $C_0 = i\,2.277$,
$C_1 = i\,0.901$, $C_2 = -i\,0.566$, $C_3 = i\,0.0163$ , $C_4 = i\,0.0344$,
$C_5 = -i\,0.009$ .
The other opto-geometrical parameters are: $\nu_1 = 1$, $\nu_2 = 1.3 + i\,7.1$, $\theta = 0°$.

Figures 12a and 12b give the efficiency curves in E// and H// polarization. These curves are not realistic because the index $\nu_2$ has been kept constant. This assumption has only been made for the sake of simplicity.

When the wavelength decreases, we must use more sources and sampling points. For that reason, routines that automatically choose the sampling points and the source location are quite useful. Figure 11 shows the points that have been used in the range $3 < \lambda < 7$. For $\lambda < 3$, the number of points has been doubled. With these values, the accuracy is better than $10^{-3}$ on each efficiency. Due to the symmetry of the profile and to normal incidence, the efficiencies in the negative orders are the same as those in the positive orders.

Table 6 gives the efficiencies for $\lambda = 2.4$. They have been computed with a greater number of sources (N = 300), and all the given digits are correct.

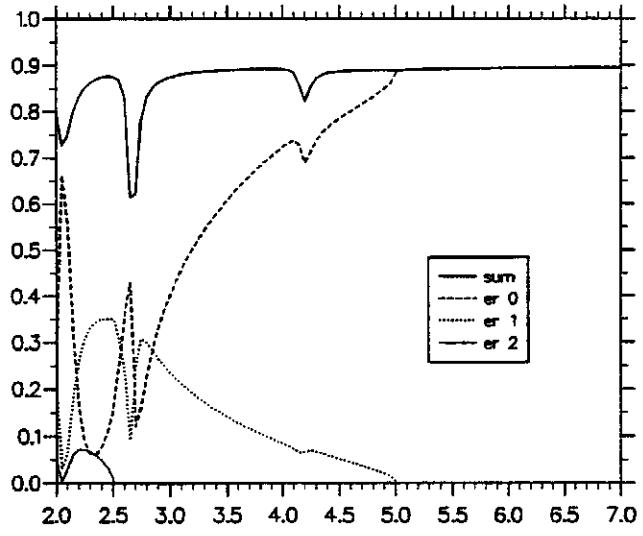


*Figure 12a. Efficiency curves and sum Σ of all the reflected efficiencies in E// polarization versus λ. For λ> 5, only the 0 order exists.*

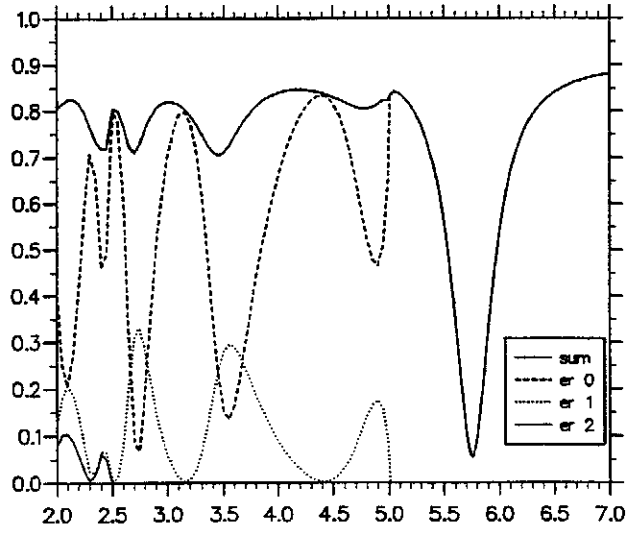


*Figure 12b. Same as figure 12a, but for H// polarization.*

| | E// | H// |
|---|---|---|
| $e_{r,-2} = e_{r,2}$ | 0.0477 | 0.0622 |
| $e_{r,-1} = e_{r,1}$ | 0.3514 | 0.0668 |
| $e_{r,0}$ | 0.0772 | 0.4604 |
| Σ | 0.8755 | 0.7183 |
| $\Delta^2$ | 2.3 E-7 | 1.2 E-8 |

*Table 6. Efficiencies for the grating of Figure 11 and $\lambda = 2.4$.*

## 4. Computation of the Green's function and of its normal derivative

The Green's function for gratings g(x,y) (41) and its derivatives are given by slow converging series (in particular for low values of y).

$$g(x,y) = \frac{1}{2id} \sum_{n \in Z} \frac{1}{\beta_n} \exp(i\alpha_n x + i\beta_n |y|) \qquad (41)$$

In this section, we describe some numerical recipes which make it possible to compute these series with good accuracy and reasonable computer time. These recipes have been used for all the computations reported in this paper. The basic idea (Kummer's transformation) is as follows: by subtracting from these series their asymptotic expansions, we get faster converging series. The method is pertinent if these asymptotic expansions can be put in closed form.

It is possible [14] to use more sophisticated asymptotic expansions as those presented here. A faster convergence can be expected. We have not yet implemented these possibilities, but they could drastically reduce the computation time.

For the sake of simplicity, we suppose in this whole section that the grating pitch d is equal to $2\pi$ (a change in the scale can easily reduce the actual problem to this one). With this assumption, Eq. (27) becomes

$$\alpha_n = \alpha_0 + n, \qquad (42)$$

and for high values of n, the asymptotic value of $\beta_n$ (Eq. (28)) is:

$$\beta_n = i|n| + i\alpha_0 \operatorname{sign}(n) + O\left(\frac{1}{n}\right) \qquad (43)$$

where sign(x) is the function equal to 1 for x>0 and to -1 for x<0.

### 4.1 Green's function

We first take off the factor $\exp(i\alpha_0 x)$ from the series in (41):

$$g(x,y) = \exp(i\alpha_0 x)\, S(x,y), \qquad (44)$$

$$S(x,y) = \frac{1}{4i\pi} \sum_{n \in Z} \frac{1}{\beta_n} \exp(inx + i\beta_n |y|). \qquad (45)$$

Let us consider the series:

$$S_\infty(x,y) = \frac{1}{4i\pi} \sum_{n\in Z^*} \frac{1}{i|n|} \exp(inx) \tag{46}$$

Using the relation (which holds true for $|z| \le 1$ and $z \neq 1$):

$$\sum_{n\in N^*} \frac{z^n}{n} = -\mathrm{Log}(1-z), \tag{47}$$

and with a good choice for the cut of the complex logarithm (this cut is also the one used by the Fortran function CLOG), $S_\infty(x,y)$ can be expressed in closed form (for $x \neq 2\pi$) by:

$$S_\infty(x,y) = \frac{1}{2\pi} \mathrm{Log}\left[2\left|\sin\left(\frac{x}{2}\right)\right|\right] \tag{48}$$

We write S(x,y) as the difference

$$S(x,y) = S_\infty(x,y) + \left[S(x,y) - S_\infty(x,y)\right], \tag{49}$$

and we put

$$\begin{aligned} S_r(x,y) &= S(x,y) - S_\infty(x,y) \\ &= \frac{e^{i\beta_0 y}}{4i\pi\beta_0} + \frac{1}{4\pi} \sum_{n\in Z^*} \left[\frac{e^{i\beta_n|y|}}{i\beta_n} + \frac{1}{|n|}\right] e^{inx} \end{aligned} \tag{50}$$

The computation of g(x,y) reduces to that of the series:

$$S_1(x,y) = \sum_{n\in Z^*} \left[\frac{e^{i\beta_n|y|}}{i\beta_n} + \frac{1}{|n|}\right] e^{inx} \tag{51}$$

This series converges faster than g(x,y), but the convergence rate can still be enhanced by putting

$$S_1(x,y) = S_2(x,y) + S_3(x,y), \tag{52}$$

$$S_2(x,y) = \sum_{n\in Z^*} \left[\frac{e^{i\beta_n|y|}}{i\beta_n} + \frac{e^{-(|n|+\alpha_0\,\mathrm{sign}(n))|y|}}{|n|}\right] e^{inx}, \tag{53}$$

$$S_3(x,y) = \sum_{n\in Z^*} \left[1 - e^{-(|n|+\alpha_0\,\mathrm{sign}(n))|y|}\right] \frac{e^{inx}}{|n|}, \tag{54}$$

The series $S_2$ converges quickly. As for $S_3$, it can be put in closed form with the help of (47):

$$\begin{aligned} S_3(x,y) = &-2\,\mathrm{Log}\left[2\sin\left(\frac{x}{2}\right)\right] + \\ &e^{-\alpha_0|y|}\,\mathrm{Log}\left(1 - e^{-|y|+ix}\right) + e^{\alpha_0|y|}\,\mathrm{Log}\left(1 - e^{-|y|-ix}\right) \end{aligned} \tag{55}$$

Finally, the computation of g(x,y) reduces to the evaluation of $S_\infty$ by (48), $S_3$ by (55), and $S_2$ by (53).

### 4.2 Derivatives of the Green's function

We consider now the partial derivatives of the Green's function. Let us first assume that $y \neq 0$ in order to ensure the convergence of the following series:

$$\frac{\partial g}{\partial x} = \frac{e^{i\alpha_0 x}}{4\pi} \sum_{n\in Z} \frac{\alpha_n}{\beta_n} \exp(inx + i\beta_n|y|) \tag{56}$$

$$\frac{\partial g}{\partial y} = \frac{e^{i\alpha_0 x}}{4\pi} \mathrm{sign}(y) \sum_{n\in Z} \exp(inx + i\beta_n|y|) \tag{57}$$

Let us call $S_4$ the series appearing in (57):

$$S_4(x,y) = \sum_{n\in Z} \exp(inx + i\beta_n|y|) \tag{58}$$

This series can be expressed as:

$$S_4(x,y) = S_5(x,y) + S_6(x,y) \tag{59}$$

$$\begin{aligned} S_5(x,y) = &\, e^{i\beta_0|y|} + \\ &\sum_{n\in Z^*} \left[e^{i\beta_n|y|} - e^{-(|n|+\alpha_0\mathrm{sign}(n))|y|}\right] e^{inx} \end{aligned} \tag{60}$$

$$S_6(x,y) = \sum_{n\in Z^*} e^{inx-(|n|+\alpha_0\mathrm{sign}(n))|y|} \tag{61}$$

After some calculations, the series $S_6$ can be put in closed form:

$$S_6(x,y) = \frac{\cosh(\alpha_0|y| - ix) - e^{-|y|}\cosh(\alpha_0|y|)}{\cosh(y) - \cos(x)} \tag{62}$$

In the same way, let us call $S_7$ the series appearing in (56):

$$S_7(x,y) = \sum_{n\in Z} \frac{\alpha_n}{\beta_n} \exp(inx + i\beta_n|y|) \tag{63}$$

Noting that the asymptotic value for large n of $\alpha_n/\beta_n$ is:

$$\frac{\alpha_n}{\beta_n} = -i\,\mathrm{sign}(n) + O\left(\frac{1}{n^2}\right), \tag{64}$$

we express this series as:

$$S_7(x,y) = S_8(x,y) + S_9(x,y) \tag{65}$$

$$\begin{aligned} S_8(x,y) = &\frac{\alpha_0}{\beta_0} e^{i\beta_0|y|} + \\ &\sum_{n\in Z^*} \left[\frac{\alpha_n}{\beta_n} e^{i\beta_n|y|} + i\,\mathrm{sign}(n)\, e^{-(|n|+\alpha_0\mathrm{sign}(n))|y|}\right] e^{inx} \end{aligned} \tag{66}$$

$$S_9(x,y) = \sum_{n\in Z^*} -i\,\mathrm{sign}(n)\, e^{-(|n|+\alpha_0\mathrm{sign}(n))|y|}\, e^{inx} \tag{67}$$

After several calculations, the series $S_9$ can be put in closed form:

$$S_9(x,y) = i\,\frac{\sinh(\alpha_0|y| - ix) - e^{-|y|}\sinh(\alpha_0|y|)}{\cosh(y) - \cos(x)} \tag{68}$$

Finally, the computation of the Green's function derivatives reduces to the evaluation of the compact terms $S_6$ and $S_9$, and the summation of the fast convergent series $S_5$ and $S_8$:

$$\frac{\partial g}{\partial x} = \frac{e^{i\alpha_0 x}}{4\pi}\left[S_8 + S_9\right] \tag{69}$$

$$\frac{\partial g}{\partial y} = \frac{e^{i\alpha_0 x}}{4\pi}\,\mathrm{sign}(y)\left[S_5 + S_6\right] \tag{70}$$

Referring to sections 2.5 and 2.6, it is worth noting that g(x,y) is the field radiated by an infinite array of currents flowing in wires which intersect the (x,y) plane at points

(m d, 0), with m integer (and $d = 2\pi$ in this section). Consequently, g(x,y) is infinitely differentiable everywhere apart from these points: Indeed, the right hand sides of (69) and (70) are continuous in this domain. In particular, replacing $S_5$ and $S_6$ by their expressions, it is easy to verify that $S_5+S_6$ vanishes for $y = 0$. On the other hand, the right hand sides of (56) and (57) diverge for $y = 0$. The reader surprised by this fact can report to any mathematical book dealing with derivation of series of functions (for $y = 0$, the convergence of series (41) is not strong enough, and the series can not be differentiated term by term).

### 4.3 Summation of the series

The summation of series (53), (60) and (66) is performed by gathering the terms +n and -n. In this way, it can be shown that we get a faster convergence. Moreover, it enables us to perform a convergence check during the computation of the series itself, and to stop the summation when a predefined accuracy is reached. We use the following criterion: three successive partial sums give three points in the complex plane; when the greater side of this triangle is less than the desired accuracy, the summation is stopped.

## 5. Conclusion

The results presented in this paper show that the method of fictitious sources (MFS) can efficiently deal with many kinds of grating profiles. In our opinion, the MFS is interesting from many points of view:

- The basic idea (represent the field in each domain of the structure as a combination of fields radiated by adequate sources) is supported by physical evidence.
- Although its theoretical justification is based on difficult problems of functional analysis, its numerical implementation does not need solid mathematical background.
- The method includes the possibility to check the accuracy of the results by means of the normalized error $\Delta$.
- Many adjustable parameters are available. For instance, we can choose the nature and the location of the fictitious sources, i.e. we can choose the basis functions for the representation of the fields.

This last feature makes the method powerful, but this freedom also leads to embarrassing situations. Some basic rules must be picked out in order to automatize the choice of the sources. We think that the results presented here can clarify this point. At the present time, we have developed automatic routines of this type in the case of wire sources. Without any doubt, the performances of the MFS could be enhanced by the combination of different kinds of sources.

At the present time, much of the computation time in our codes is devoted to the calculation of the Green's function and its derivatives. The algorithms used for these computations are still not perfect, and the implementation of the ideas presented in [14] could probably drastically reduce the computation time.

## 6. References


[1] R. Petit, Editor, *Electromagnetic Theory of Gratings*, Topics in Current Physics, Vol.22, Springer-Verlag, Berlin, 1980

[2] M. Cadilhac, R. Petit, "On the diffraction problem in electromagnetic theory: a discussion based on concepts of functional analysis including an example of practical application", *Huyghens' Principle 1690-1990, Theory and Applications*, Edited by H. Block, H.A. Ferwerda, H.K. Kuiken, Elsevier Science Publishers B.V., p.249-272, 1992

[3] G. Tayeb, Thèse de Doctorat en Sciences, Université d'Aix-Marseille III, 1990

[4] G. Tayeb, R. Petit, M. Cadilhac, "The synthesis method applied to the problem of diffraction by gratings: the method of fictitious sources", SPIE, Vol.1545, International Conference on the Application and Theory of Periodic Structures, p.95-105, 1991. ISBN 0-8194-0673-2

[5] Y. Leviatan, A. Boag, "Analysis of electromagnetic scattering from dielectric cylinders using a multifilament current model", IEEE Trans. Ant. Prop., Vol. AP-35, N.10, p.1119-1127, 1987

[6] A. Boag, Y. Leviatan, A. Boag, "Analysis of two-dimensional electromagnetic scattering from a periodic grating of cylinders using a hybrid current model", Radio Science, Vol.23, N.4, p.612-624, 1988

[7] A. Boag, Y. Leviatan, A. Boag, "Analysis of diffraction from echelette gratings, using a strip-current model", J. Opt. Soc. Am. A, Vol.6, N.4, p.543-549, 1989

[8] A. Boag, Y. Leviatan, "Analysis of two-dimensional electromagnetic scattering from nonplanar periodic surfaces using a strip current model", IEEE Trans. Ant. Prop., Vol.37, N.11, p.1437-1446, 1989

[9] C. Hafner, *The Generalized Multipole Technique for Computational Electromagnetics*, Artech House Books, Boston, 1990

[10] C. Hafner, "Efficient MMP Computation of Periodic Structures", ACES' 94 Conference Proceedings, 1994

[11] J.A. Kong, *Electromagnetic Wave Theory*, Wiley-Interscience Publication, New York, 1986

[12] W. Press, S. Teukolsky, W. Vetterling, B. Flannery, *Numerical Recipes*, Cambridge University Press, 1992

[13] D. Maystre, " A new general integral theory for dielectric coated gratings", J. Opt. Soc. Am., Vol.68, N.4, p.490-495, 1978

[14] N. Nicorovici, R. McPhedran, R. Petit, "Efficient calculation of the Green's function for electromagnetic scattering by gratings", to be published in Phys. Rev. B